DOI 10.1007/s10812-018-0578-8
*Journal of Applied Spectroscopy, Vol. 84, No. 6, January, 2018 (Russian Original Vol. 84, No. 6, November–December, 2017)*

# SYNTHESIS OF NICKEL–CARBON NANOPARTICLES BY ELECTRICAL DISCHARGE IN LIQUID

**V. S. Burakov,[a] V. V. Kiris,[a] A. A. Nevar,[a] M. I. Nedelko,[a] N. V. Tarasenko,[a*] and G. N. Churilov[b]**

UDC 537.52;535.338.35;533.9.08

*Composite nickel–carbon nanoparticles were synthesized by electrical discharge in liquid. The synthesis was carried out in water and ethanol under various discharge conditions, including purging the discharge gap with argon. In water, electrical discharge was conducted between graphite and nickel electrodes. In ethanol, two nickel electrodes were used with the liquid acting as the carbon supplier. The size of the particles obtained, their composition, and the production rate depend on the type of working fluid and synthesis duration. It was also shown that the particle production rate in water is greater than in ethanol, and purging the electrode gap with argon reduces this rate two or three times.*

***Keywords:*** *electrical discharge in liquid, nickel–carbon nanoparticle.*

**Introduction.** Group VIII transition metals, such as Ni, Fe, and Co, can be a good alternative to noble metals in catalysis of various chemical processes [1, 2], in particular, oxidation of carbon monoxide and propane [3]. In addition, due to high magnetization, the nanoparticles (NP) of these metals are of interest for the development of magnetic carriers of high-density information, the synthesis of ferromagnetic liquids, and magnetic resonance imaging [4]. Transition metal oxides in composites with graphene are also widely studied as a promising material for increasing the capacity of electric storage devices (so-called supercapacitors) [5].

The main problem with the use of these metals is their high reactivity, in particular, the sensitivity to oxidation in air, even at room temperature. In addition, metal NPs are prone to aggregation. It is known that the stabilization of metallic NPs can be carried out by coating them with organic molecules, polymers or oxides, but these types of coatings are dielectrics and can reduce the efficiency of charge transfer between NPs and reagents, thereby reducing their catalytic activity. To use NPs as a catalyst, the passivation layer should stabilize the metal NP in the reaction medium and provide the necessary level of electrical conductivity [1, 6]. The solution of these problems is important for the use of NPs in other areas.

Carbon can be an effective passivation layer to prevent oxidation of transition metals because oxidants cannot diffuse through its lattice. Carbon itself is chemically inert in a wide temperature range and has a high electrical conductivity. Thus, the synthesis of composite metal–carbon NPs, particularly metallic NPs coated with a carbon shell or encapsulated in a carbon matrix, is of particular interest, since the carbon shell can prevent their chemical degradation due to the environment, and prevents agglomeration while ensuring efficient functionalization [1, 6, 7].

An electric discharge in a liquid is an easy and effective method for synthesizing nanostructures of metals and complexes based on them [4, 6–8]. Despite a large number of publications on this subject, the principal mechanisms for the formation of NPs by electrical discharge in a liquid remain not fully understood. To meet the requirements for NPs used in specific applications, it is necessary to understand the synthesis mechanisms and methods of its control in order to obtain particles with specific properties.

This work is a result of the project for investigating the formation of metal–carbon nanostructures in electrical discharge plasma and determining their properties. The properties of composite nickel–carbon NPs synthesized by electrical discharge in water and ethanol under various discharge regimes are discussed. It is shown that the size of the obtained NPs, their composition and the rate of NP production depend on the nature of the working fluid and on synthesis duration.

*To whom correspondence should be addressed.

[a]B. I. Stepanov Institute of Physics, National Academy of Sciences of Belarus, 68-2 Nezavisimost′ Ave., Minsk, 220072, Belarus; email: tarasenko@ifanbel.bas-net.by; [b]L. V. Kirensky Institute of Physics, Siberian Branch of the Russian Academy of Sciences, Krasnoyarsk, Russia. Translated from Zhurnal Prikladnoi Spektroskopii, Vol. 84, No. 6, pp. 927–935, November–December, 2017. Original article submitted September 4, 2017.

TABLE 1. Description of the Test Samples

| No. | Electrodes | Working fluid | Purge | Color of the colloidal solution |
|---|---|---|---|---|
| 1 | Ni–C | Water | — | Black; transparent light brown after settling |
| 2 | Ni–C | Water | Ar | Black; transparent light brown after settling |
| 3 | Ni–Ni | Ethanol | — | Black; transparent brown after settling |
| 4 | Ni–Ni | Ethanol | Ar | Black; black after settling |

**Setup and Conditions for the Synthesis of NPs.** The design of the reactor for the synthesis of NPs by electrical discharge, as well as the method for determining the electrical and spectroscopic parameters of the discharge, are described in detail in [9]. The experimental system was based on a high-voltage pulse generator with controlled capacitance, inductance, and ballast resistance. The discharge was carried out in a fluoroplastic chamber with two quartz windows for optical diagnostics of the plasma. The reactor chamber module was equipped with an electrode holder for adjusting the electrode gap and rotating one of the electrodes. A system for supplying the working liquid and gas to the reactor chamber was included. The gas was fed into the electrode gap through an opening ~1 mm in diameter, cut along the axis of one of the electrodes. The experimental setup provided for control of the electrical and spectroscopic characteristics of the plasma. The current–voltage characteristic of the discharge was recorded by a digital oscilloscope using a Rogowski coil and a voltage divider.

A fundamental feature of the experimental system was the possibility of purging the electrode gap with an inert gas (argon), which extends the possibilities of controlling the synthesis process. Purging the electrode gap with argon makes the discharge occur in the gaseous medium, leading to a substantial increase in the emission intensity of the spectral lines and a radical decrease in continuous radiation [9]. The significant increase in temperature due to the transition to the purge mode is quite natural, since in the presence of purging the discharge occurrs in a substantially less dense medium with a smaller mass of material involved in the discharge, and also with a higher effective ionization potential of the plasma [9].

In order to optimize the parameters of the synthesized particles, production conditions were varied. In all experiments on the synthesis of nickel–carbon particles, the current in the primary winding of the transformer was 1.4 A, capacitance was 5 nF, breakdown voltage was ~12 kV, the volume of liquid in the reactor chamber was 200 mL. In water, the discharge was conducted between a nickel and graphite electrode. An increased inductance discharge circuit (150 μH) was installed in order to avoid mechanical destruction of the graphite electrode by hydraulic impact. In an aqueous environment, electrical discharge regimes with and without purging the electrode gap with argon were worked out. In the case when an argon purge was employed, flow rate of argon was 0.2 $m^3/h$, which is sufficient for stable displacement of liquid from the electrode gap and initiation of the discharge in the gaseous medium.

In the synthesis of NPs, the source of the initial elements can be not only the electrode material, but also the liquid itself [2, 10]. At the same time, rapid nonuniform mechanical destruction of the graphite electrode during discharge in liquid makes it difficult to maintain a constant electrode gap. In addition, the solution is contaminated with a large number of coarse particles from the graphite electrode. This problem can be solved by using two nickel electrodes and replacing water with a carbon-containing liquid. Ethanol was chosen as the carbon-containing liquid. Production of particles in ethanol was carried out with and without purging the electrode gap with argon at a controlled flow rate.

NPs were obtained by the electric discharge method with the formation of a colloidal solution. For further studies, the solutions were allowed to settle for 1 h to remove large particles formed as a result of mechanical destruction of the electrodes. Then the colloid was poured into another container, except for the last 10 mL containing large sediment particles on the bottom. The conditions for the synthesis of nickel–carbon particles and the qualitative description of colloidal solutions are given in Table 1.

**Research Methods.** The shape and size of synthesized nanostructures were evaluated by transmission electron microscopy (TEM). For this, ~2–3 μL of a colloidal solution were pipetted onto a copper mesh covered with a formvar film and stabilized with carbon. After applying the sample to the substrate, it was left in air to dry completely. Microphotographs of NPs were obtained on an LEO 906E electron microscope (LEO, UK, Germany) at a maximum accelerating voltage of 160 kV.

For X-ray diffraction studies on a DRON-3M X-ray diffractometer, the samples were formed on a glass substrate by repeatedly applying a 50 μL drop of colloidal solution and drying it at room temperature. The phase composition

of the obtained films was identified from the angular dependences of the diffraction peak intensities of scattered radiation on the Cu$K_\alpha$ copper line ($\lambda$ = 0.15418 nm) in the range of 10–90$^o$ angles.

Initial control of the composition and structure of the products formed was carried out by measuring their Raman spectra. The Raman spectra were recorded with a Spectra Pro 500i spectrometer (Action Research Corporation, USA) operating at the second harmonic of a YAG:Nd laser ($\lambda$ = 532 nm, 30 mW power) in a backscattering configuration with a spectral resolution of 1 cm$^{-1}$.

The samples were analyzed by IR spectroscopy in the external specular reflection regime. Colloids of the particles produced were applied to aluminum foil, the reflection coefficient of which is close to 100% in the investigated spectral range (400–4000 cm$^{-1}$), and dried at room temperature. IR spectra were measured using a Nexus IR Fourier transform spectrometer (Thermo Scientific, USA) with a spectral resolution of 0.1 cm$^{-1}$ and a maximum SNR of 33,000:1.

The concentration of electrode material in the solution was determined using an iCap Q inductively coupled plasma mass spectrometer (Thermo Scientific). The following sample preparation procedure was used in the analysis. An aliquot of the solution (2 mL) was transferred to a 200-mL flask by means of a calibrated pipette, 50 mL of deionized water (resistivity 18 MΩ/cm) and 10 mL of nitric acid (ACS purity) were added, the solution was stirred and topped off with deionized water to the required volume. To optimize the measurement mode and minimize possible interference, the position of the burner, ion optics and detector were tuned using the standard software of the spectrometer with the Thermo Scientific Tune B standard solution. For the measurements, Ni 60 was the selected isotope because it provides the best sensitivity and reproducibility of measurements. Quantitative analysis of the samples was conducted based on a calibration curve for this isotope constructed for a standard nickel solution in the concentration range of 0.1–3.0 mg/L. Each sample was measured three times, the results of the measurements were averaged. Elemental composition of the accumulated NPs was determined using a standard-free laser spectral analysis [11, 12].

**Results and Discussion.** An electric discharge between two electrodes immersed in a liquid is accompanied by the formation of a rapidly expanding luminous plasma-bubble, inside of which the material melts and evaporates from the surface of the electrodes. When discharged in water, graphite electrode served as the carbon source. When discharged in alcohol, ethanol decomposition products formed in the plasma channel and at the contact interface of the liquid vapor with the products of nickel electrode erosion served as the source of carbon.

In the course of the discharge, the solution gradually lost its transparency and turned black. After settling for 1 h, the colloidal solutions synthesized while purging with argon became transparent, while retaining a light brown color. The solutions prepared without purging remained black and opaque. Despite the small sediment due to particle aggregation, the obtained solutions remained stable for a week or even several months (in the case of a discharge between nickel electrodes in ethanol).

The obtained TEM images of NPs synthesized for 5 min are shown in Fig. 1. It can be seen that the synthesized material consists of rather small spherical NPs assembled into aggregates, which, most likely, does not result from a large concentration of particles in the solution. With a great deal of certainty, it can be argued that the formation of agglomerates occurs when the solution dries on the mesh, since the prepared slurries remain stable for a long time without precipitation or clouding of the solution. The dark and light contrast of TEM images of NPs suggests a different phase composition of the substance. Thus, the gray area around the darker particles indicates that the nickel NPs are encapsulated in carbon and/or oxide shells. It was possible to estimate the dimensions of the NPs from the combined set of micrographs (Fig. 1, inserts). The average size of the NPs was in the range of 2–3 nm. No significant difference in size of the NPs is perceptible in the obtained micrographs.

A somewhat different picture is observed with an increase in the synthesis duration. On the microphotographs (Fig. 2) of particles obtained by electrical discharge in 20 min, large particles ~40–80 nm in size are seen in the case of a discharge between graphite and nickel electrodes in water without purging, and when purging with argon, the produced particles are 15–20 nm in size. At the same time, they are assembled into aggregates, which is probably a consequence of the high concentration of particles in the solution. For synthesis in alcohol, an increase in the synthesis duration also results in an increase in the size of the NP — to 4–6 nm without purging and up to 5–10 nm when purging with argon. In addition, single submicron core-shell type particles are encountered in the solution (Fig. 2c, d, insets); their size is ~500 nm, the shell thickness varies within the range of 20–40 nm. On TEM images it can be seen that the color of the core is black, and the shells are light gray. It can be assumed, and the results of energy-dispersive X-ray spectroscopy to a large extent confirm this (Fig. 2d, e), that the core of the particle consists of metallic nickel, and the shell is either a consequence of nickel oxidation on the surface or a layer/layers of deposited carbon. Table 2 presents generalized results of the study of particle size by TEM.

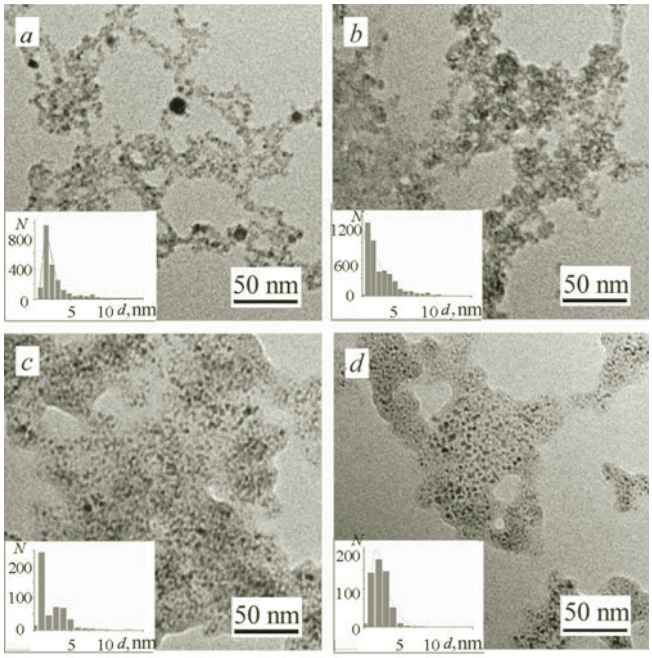


Fig. 1. TEM images and distribution histograms (see insets) of nickel–carbon nanoparticles synthesized by electrical discharge between Ni–C electrodes in water without purging (a) and purging with Ar (b), between Ni–Ni electrodes in ethanol without purging (c) and purging with Ar (d).

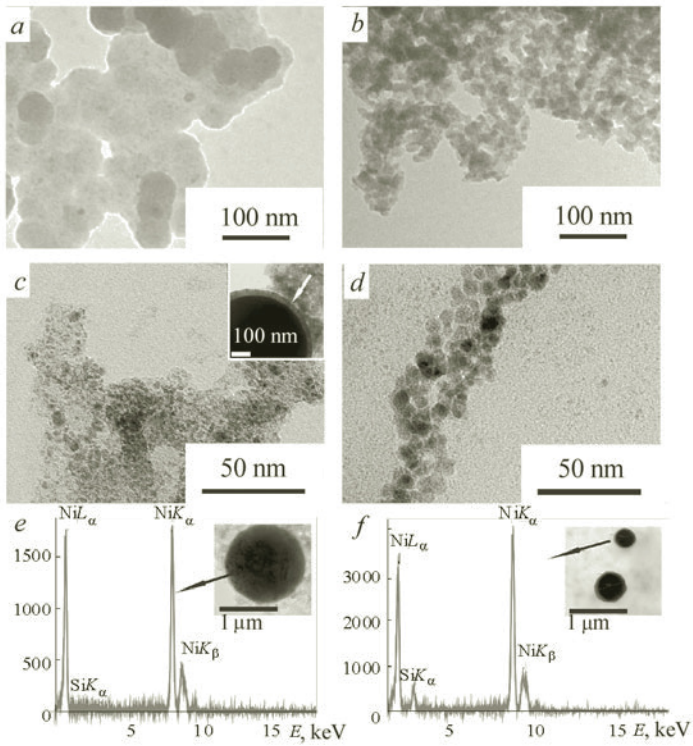


Fig. 2. TEM images of nickel–carbon nanoparticles obtained in 20 min by synthesis between Ni–C electrodes in water without purging (a) and purging with Ar (b), between Ni–Ni electrodes in ethanol without purging (c) and purging with Ar (d); e, f) results of the composition analysis of submicron particles (see insets) by energy dispersive X-ray spectroscopy.

TABLE 2. Results of Particle Size Investigations

| No. | Electrodes | Working fluid | Purge | Synthesis time, min | Nanoparticle size, nm |
|---|---|---|---|---|---|
| 1 | Ni–C | Water | — | 5 | 2–3 |
| | | | | 20 | 40–80 |
| 2 | Ni–C | Water | Ar | 5 | 2–3 |
| | | | | 20 | 15–20 |
| 3 | Ni–Ni | Ethanol | — | 5 | 2–3 |
| | | | | 20 | 4–6 |
| 4 | Ni–Ni | Ethanol | Ar | 5 | 2–3 |
| | | | | 20 | 5–10 |

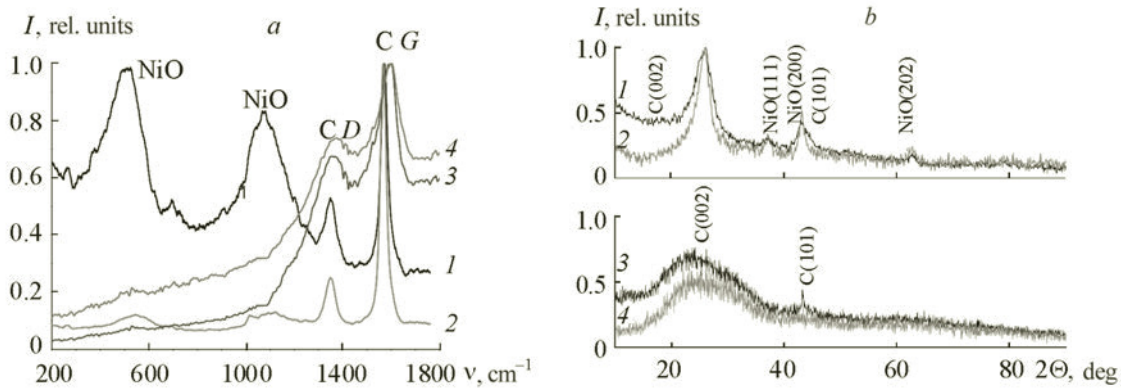


Fig. 3. Raman spectra (a) and diffraction patterns (b) of nanoparticles synthesized by electric discharge between Ni–C electrodes in water without purging (1) and purging with Ar (2), between Ni–Ni electrodes in ethanol without purging (3) and purging with Ar (4).

In Raman spectra of particles synthesized in water between nickel and graphite electrodes, both *D*- and *G*-bands of carbon, as well as nickel oxide bands, are visible (Fig. 3a, curves 1, 2). The *D*-band, located in the 1300–1350 $cm^{-1}$ spectral range and characteristic of carbon structures, associated with disordered carbon, was measured at 1348, 1351, 1358, and 1377 $cm^{-1}$ for samples 1–4, respectively. The *G*-band, responsible for $sp^2$-hybridized carbon is observed at 1566 $cm^{-1}$ for Ni–C samples synthesized in water, and at 1598 $cm^{-1}$ for Ni–Ni samples synthesized in ethanol. The shift and broadening of the Raman bands of nickel oxide confirm the small size of the formed NPs. In the case of synthesis of particles in alcohol, nickel oxide bands are absent, only peaks characteristic of carbon are present (curves 3, 4). In addition, in the samples synthesized in ethanol, there is a significant broadening of the *D*- and *G*-peaks. Such a spectrum is characteristic of amorphous carbon [13, 14]. When synthesized in water, the nature of the Raman spectrum changes, the bands become narrower and their overlap decreases. Also, the intensity of the *D*-band decreases, and of the *G*-band, on the contrary, increases, which is characteristic of graphite. The level of graphitization is usually characterized by the ratio of the intensities of the *D* and *G* bands ($I_D/I_G$), which in our case for Ni–C samples synthesized in water without purging is 0.7, and when purging with argon is 0.3, and for Ni–Ni samples synthesized in ethanol without purging, $I_D/I_G = 1.6$, and when purging with argon it is 1.9. Intensity of the bands was measured by the Lorentz approximation of the spectral profile. The decrease in the $I_D/I_G$ ratio points to an increase in the degree of graphitization of carbon samples. The position of the *G*-band depends on the size of the crystallites, and the observed shift toward higher frequencies reflects a decrease in the crystallite size and an increase in the number of defects. The higher intensity of the *G*-band for samples synthesized in water with a graphite electrode indicates that the amount of structurally ordered carbon exceeds the amount of amorphous and unordered carbon.

Figure 3b shows the results of X-ray structural analysis of synthesized samples. Diffractograms of particles synthesized in water contain reflections of nickel oxide and graphite, and in the case of synthesis in ethanol, mainly peaks characteristic of carbon can be seen. In the case of a discharge between nickel electrodes in ethanol without purging

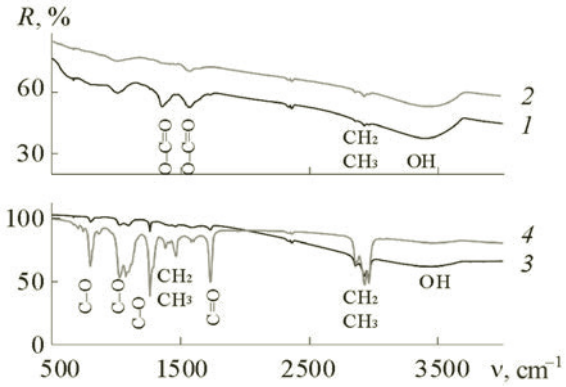


Fig. 4. IR spectra of nickel–carbon nanoparticles produced: between Ni–C electrodes in water without purging (1) and purging with Ar (2); between Ni–Ni electrodes in ethanol without purging (3) and purging with Ar (4).

the discharge gap with argon, the diffractograms contain two broad reflections at diffraction angles $2\Theta = 26.58$ and $42.41^{o}$, which correspond to the (002) and (101) planes of hexagonal graphite [15]. Without purging, one broad reflection is observed at the diffraction angle of $26.42^{o}$, and there is a weak narrow peak, which can be attributed to metallic nickel in accordance the results of energy-dispersive X-ray spectroscopy analysis. It is possible that the absence of pronounced peaks corresponding to metallic nickel or its oxide is due to small size of particles and the presence of defects in their structure. The X-ray diffraction method is known to be sensitive only to larger ordered structures.

Taking into account the obtained IR spectroscopy and X-ray diffraction data (Fig. 3), it is possible that in the case of synthesis in both water and ethanol, the obtained samples consist of fine particles (Fig. 1), most likely metallic nickel in the case of synthesis in ethanol and/or nickel oxide in the case of synthesis in water. The particles are surrounded by a shell, which, according to the Raman spectrum (Fig. 3a), consists of graphite in the case of synthesis in water, and from amorphous carbon in the case of ethanol. The carbon envelope protects the NPs synthesized in ethanol from oxidation in air when they are applied to a substrate.

**Determination of the Composition of Functional Groups on the Surface of the Particles.** Implementation of unique characteristics of NPs in specific applications requires specific properties. For example, the use of nanofillers in polymer composites requires the affinity of NPs for fillable matrices, medical applications demand biocompatibility, and to be effectively used in catalysis, NPs must be able to adsorb precursors. These properties largely depend on the composition of the substance sorbed on the surface of the particle, which is critically important for their effective functionalization.

The composition of the functional groups on the surface of NPs was determined using FTIR spectroscopy. The measured spectra are shown in Fig. 4. It can be seen that the composition of functional groups on the surface of NPs depends essentially on the composition of the liquid, in which the production takes place. In the spectrum of particles synthesized by electric discharge in distilled water, the bands of hydroxyl and carboxyl groups (–OH, –COOH) are clearly pronounced; the bands of methyl ($–CH_3$) and methylene ($–CH_2$) groups are very weak. This is consistent with the diagnostic data of discharge plasma in water, which demonstrate a high oxygen content [9]. Synthesis in ethanol leads to the formation on the surface of particles of compounds with a large number of methyl and methylene groups; carbonyl and hydroxyl groups are also present. Qualitatively, the composition of the groups on the particle surface in the case of synthesis in ethanol corresponds to the groups present in ethanol itself (with the exception of carbonyl group), but on the whole the spectrum differs markedly from the spectrum of ethanol, i.e., the structure of the groups formed differs from the structure of ethanol.

**The Rate of Particle Production in Different Modes.** The efficiency of NP production in various operating modes of the reactor was determined from nickel concentration in the solution using inductively coupled plasma mass spectrometry. The results of measurements are given in Table 3. As can be seen, the purging of the electrodes reduces the rate of production by a factor of ~2.5. This is not related to the possibility of removing some of the produced material by the flow of argon. As additional measurements show, the purge carries away an insignificant amount of material (<1% of the total produced amount). The decrease in particle production rate when purge is employed can be associated with a higher degree of localization of the discharge channel in the breakdown of liquid compared with gas, which provides a higher current density and more efficient erosion of the electrode material, in spite of the significantly higher energy costs for breakdown and heating of the denser environment.

TABLE 3. Results of Measuring Nickel Concentration in Samples and Determining Particle Production Rate

| Operating mode of the reactor | Concentration of Ni in the solution after operating for 5 min, mg/dm$^3$ | Ni production rate, mg/min |
|---|---|---|
| Water, Ni–C electrodes | 21.4 | 0.86 |
| Water, Ni–C electrodes, argon purge | 8.6 | 0.34 |
| Ethanol, Ni–Ni electrodes | 13.9 | 0.56 |
| Ethanol, Ni–Ni electrodes, argon purge | 5.6 | 0.22 |

TABLE 4. Plasma Parameters and Relative Concentration of Elements in Discharge Plasma and in Samples

| Discharge parameter | Ni–C, water | Ni–C, water, Ar | Ni–Ni, ethanol | Ni–Ni, ethanol, Ar |
|---|---|---|---|---|
| Temperature, eV | 1.38 | 1.46 | 1.33 | 1.41 |
| $N_e$, $10^{17}$ cm$^{-3}$ | 20.8 | 9.04 | 22.7 | 11.5 |
| Molar ratio of elements to nickel, Ni:O:C:Ar:H | 1<br>22.1<br>4.2<br>0<br>61.3 | 1<br>4.6<br>1.8<br>2.7<br>11.9 | 1<br>13.2<br>30.6<br>0<br>76.5 | 1<br>1.9<br>6.8<br>3.5<br>18.7 |
| Ni:C molar ratio | 1:3.8 | 1:3.2 | 1:6.9 | 1:9.4 |

Another possible mechanism for increasing the production efficiency of the desired product by discharge directly in a liquid can be associated with the action of a dense inhomogeneous plasma with high temperature and pressure gradients on the surface of the electrode, leading to "spattering" of the melt of the electrode material and, as a consequence, the formation of submicron droplets. The existence of such a mechanism, which is not associated with the condensation of the evaporated material, is indicated by the difference in the composition of plasma and the particles produced.

The composition of the discharge plasma was determined from an analysis of its emission spectra by the method described in [9] using the basic relationships of optical emission spectroscopy. The temperature of electric discharge plasma was determined by the oxygen line groups O I 795 nm and O I 844.6 nm, each of which consists of three lines with close excitation potentials. The energy of the upper level, the transition probabilities and the degeneracy of the lines were taken from the Harvard–Smithsonian Center for Astrophysics database. To improve the accuracy of measurements of the integrated line intensity, the lines were approximated by the Voigt profile. Electron concentration was determined from the width of the carbon line C I 833.5 nm, the broadening constants were taken from [16]. Since the measurements were carried out in air, the lines of oxygen and nitrogen were not taken into account in the calculations, and the ratio of carbon to nickel was calculated from the lines C I 833.5 nm and Ni I 761.7 nm.

The rate of nickel production in ethanol is slightly less than in water, despite the fact that discharge in ethanol is performed using two nickel electrodes, whereas discharge in water is performed with one graphite and one nickel electrode. One of the reasons may be that ethanol decomposes more easily, saturating the discharge plasma with decomposition products, which require more energy to heat up. This is confirmed by the plasma discharge diagnostic data: Table 4 shows that the relative fraction of the electrode material in an electric discharge plasma in ethanol is lower than in water. The difference in the nickel/carbon molar ratios in the samples and in the discharge plasma suggests that besides condensation, other mechanisms of formation of NPs take place. It should be noted that for the discharge occurring directly in liquid without purging, the relative magnitude of this difference is greater.

**Conclusions.** Using the methods of transmission electron microscopy, X-ray diffraction, Raman spectroscopy, and FTIR spectroscopy, the structural and morphological characteristics of nickel–carbon nanoparticles formed in electric discharge plasma in water and ethanol were determined with and without purging the electrode gap with argon. The developed simple one-stage method can be used to produce nickel nanoparticles embedded in a carbon and/or oxide matrix. Such structures are undoubtedly of interest for use as catalysts, as well as for creating protective layers for microwave devices.

The presence of organic groups such as –OH, –COOH, etc., on the surface of synthesized particles permits successful functionalization of their surface for biomedical applications.

**Acknowledgment.** The study was carried out within the framework of the joint project of the Belarusian Republican Foundation for Fundamental Research and the Siberian Branch of the Russian Academy of Sciences (project F15SO-013 "Investigation of the Formation of Metal-Carbon and Intermetallic Nanostructures in Electric Discharge Plasma, Production Methods, and Properties").

## REFERENCES

1. C. Wang, P. Zhai, Z. Zhang, Y. Zhou, J. Zhang, H. Zhang, Z. Shi, R. Han, F. Huang, and D. Ma, *J. Catalysis*, **334**, 42–51 (2016).
2. A. L. M. da Silva, J. P. den Breejen, L. V. Mattos, J. H. Bitter, K. P. de Jong, and F. B. Noronha, *J. Catalysis*, **318**, 67–74 (2014).
3. Yu. G. Morozov, O. V. Belousova, and M. V. Kuznetsov, *Inorg. Mater.*, **47**, 36–40 (2011).
4. K. H. Ang, I. Alexandrou, N. D. Mathur, G. A. J. Amaratunga, and S. Haq, *Nanotechnology*, **15**, 520–524 (2004).
5. N. B. Trung, T. V. Tam, D. K. Dang, K. F. Babu, E. J. Kim, J. Kim, and W. M. Choi, *Chem. Eng. J.*, **264**, 603–609 (2015).
6. M. R. Sanaee and E. Bertran, *J. Nanomater.*, 450183 (10 p.) (2015).
7. S. Chaitoglou, M. Reza Sanaee, N. Aguiló-Aguayo, and E. Bertran, *J. Nanomater.*, 178524(1–8) (2014).
8. G. Saito and T. Akiyama, *J. Nanomater.*, 123696 (21p.) (2015).
9. V. S. Burakov, V. V. Kiris, A. A. Nevar, M. I. Nedelko, and N. V. Tarasenko, *Zh. Prikl. Spektrosk.*, **83**, No. 4, 633–639 (2016) [V. S. Burakov, V. V. Kiris, A. A. Nevar, M. I. Nedelko, and N. V. Tarasenko, *J. Appl. Spectrosc.*, **83**, No. 4, 643–649 (2016)].
10. N. Parkansky, O. Goldsmith, B. Alterkop, R. L. Boxman, Z. Barkay, Yu. Rosenberg, and G. Frenkel, *Powder Technol.*, **161**, 215–219 (2006).
11. V. S. Burakov and S. N. Raikov. *Spectrochim. Acta, B: At. Spectrosc.*, **62**, 217–223 (2007).
12. E. Tognoni, G. Cristoforetti, S. Legnaioli, and V. Palleschi, *Spectrochim. Acta, B: At. Spectrosc.*, **65**, 1–14 (2010).
13. A. C. Ferrari, *Solid State Commun.*, **143**, 47–57 (2007).
14. C. J. Reckmeier, J. Schneider, A. S. Susha, and A. L. Rogach, *Opt. Express*, **24**, A312–A340 (2016).
15. International Centre for Diffraction Data, form 08-0415.
16. G. Grim, *Spectral Line Broadening in Plasma* [in Russian], Mir, Moscow (1978).